

Laser Micro Machining of Alumina by a Picosecond Laser

Eric Gärtner^{*1}, Vittorio Polise^{*2}, Flaviana Tagliaferri^{*3} and Biagio Palumbo^{*2}

^{*1} *Fraunhofer - Institute for Machine Tools and Forming Technology IWU, Chemnitz, Germany*

^{*2} *University of Naples Federico II, Department of Industrial Engineering, Naples, Italy*

^{*3} *Technische Universität Chemnitz, Institute for Machine Tools and Production Processes (IWP), Chemnitz, Germany*

In the present study aluminium oxide (Al_2O_3) has been micro structured through laser milling process using a Nd:YVO₄ picosecond laser. A statistical approach based on Design of Experiments (DoE) has been successfully adopted with aim to detect which and how the process parameters affect the process as well as to explain the effect of the process parameters on the material removal rate and surface quality. The analysed parameters were scanning speed (Ss), power and line distance (i.e. the distance of two consecutive scan lines). The response variables were material removal rate and surface roughness. The ANalysis Of VAriance (ANOVA) has been applied to the results analysis. In order to understand the influence of main parameters and their interactions on the response variables, a Central Composite Design (CCD) has been chosen and performed successfully.

DOI: 10.2961/jlmn.2018.02.0005

Keywords: Picosecond laser, micro structuring, alumina, aluminum oxide, design of experiments, DOE, Central Composite Design

1. Introduction

Nowadays ceramic materials are used for several applications in different fields such as electronic, mechanical, automotive, defence and medical industries. As there is a growing need of high performance ceramics (e.g. alumina) research tests the processing and manufacture of such materials increasingly, how confirmed in [1]. The growing interest in ceramic materials is linked with their properties. In fact, they are refractory and resistant at high temperature. Moreover, ceramic materials are characterised by high hardness, low density, good compressive strength, wear resistance, lower thermal and electrical conductivity as well as chemical stability. However, due to its brittle and high-tensile material behavior, the processing of high performance ceramic with conventional cutting processes is classified as demanding because of the lower material removal rate (MRR), high tool wear and high production costs [2]. Many authors investigated and proposed different non-conventional manufacturing processes for machining of advanced ceramic, such as Electrical Discharge Machining (EDM) or Abrasive Water Jet (AWJ) [3-9]. Indeed, these are partly associated with a considerable technical effort (EDM) or cause other difficulties such as cracking [7] and high surface roughness [8].

Laser milling has several advantages compared to conventional machining methods, such as: high flexibility in shaping and working material, contactless material removal, no tool wear and environmental friendliness [1]. Furthermore, the efficient control of depth and amount of energy is beneficial. This technology is suitable for micro structuring due to its lateral resolution, low heat input and small beam diameter, as well as observed in [10]. But, according to [9], there exists a general conflict between precision and efficiency in laser micro structuring.

In this study, laser ablation was carried out on aluminium oxide using a Nd:YVO₄ picosecond laser. A statistical

approach based on DoE was adopted and the ANOVA has been applied to the results analysis. In order to understand the influence of main parameters and their interactions on the response variables, a CCD has been chosen and performed successfully. By means of this approach it is possible to find out a statistical model of the response variable behaviour changing process parameters. This paper will present the results of the investigation which aimed to reduce the process time while maintaining or improving manufacturing accuracy and surface roughness.

2. Materials and Equipment

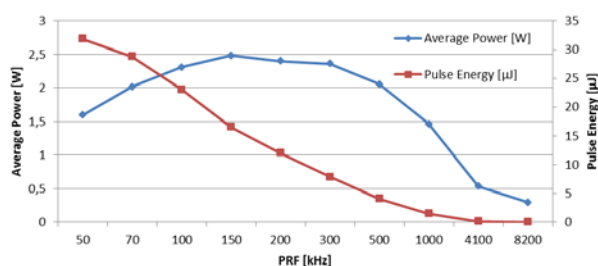
The machined material in the case study was commercial aluminum oxide Al_2O_3 at 96 %. It belongs to the family of ceramic materials.

The experiments here presented have been carried out with a Nd:YVO₄ picosecond laser. For that, the laser microstructuring machine: Acsys Barracuda μ Custom by Acsys Lasertechnik GmbH has been used. The laser beam was positioned by an xy-galvanometer-scanner and focused on the workpiece surface by a flat field objective. The computer controlled laser system allows the setup of the process parameters. Detailed characteristics of the laser system are shown in table 1.

By the used laser, pulse energy (Pe) and average power are dependent on pulse repetition frequency (PRF), as shown in figure 1. The average power was measured using a power meter (PM-USB PM150-50C by COHERENT).

Table 1 Laser system characteristics.

Characteristics	Value	Unit
Wavelength	532	[nm]
Seed laser repetition rate	82.02	[MHz]
Pulse repetition frequency (PRF)	50÷8200	[kHz]
Pulse duration	12	[ps]
Average output power (at PRF = 70 kHz)	2.02	[W]
Scanning speed	1÷2000	[mm/s]
Beam quality factor M^2	< 1.3	-
Focused spot diameter	10.6	[μm]

**Fig. 1** Average power and pulse energy vs. pulse repetition frequency (PRF) for 532 nm by $P_{\%} = 100\%$.

The pulse energy decreases with increasing frequency. The same applies to the average power which decreases after reaching its maximum at 150 kHz. Pulse energy and pulse power determine the fluence (energy density) and the irradiance (power density) and thus the amount of machined volume. Consequently, they play a central role in laser machining and micro machining [1, 12-17].

Residual surface features, the ablation rate, and the residual surface roughness were determined by 3D-laser scanning microscopy Keyence VK-9700 and scanning electron microscopy (SEM) Leo 1455 VP. The nature of the ablation debris was investigated with SEM and energy dispersive X-ray spectroscopy (EDX) analysis system INCA.

3. Experimental Design

In order to decrease the process time and to explain the effect of the process parameters on the ablation rate and surface quality, a statistical approach based on Design of Experiment has been adopted.

For an appropriate statistical approach, a pre-experimental planning phase is required. Following the systematical planning proposed in [18-19] and applied in [1, 8, 9], a pre-design guide sheets were drawn up. The latter had been drawn with preliminary steps and relevant background [1, 19-22].

Two experimental testing series were executed. In the first step the activity has been focused on research of critical process parameters, the operating window of the process and the levels to be adopted in the final experimental phase. Therefore, preliminary tests were executed changing the process parameters in the range of the settable values for the adopted laser system. These tests were performed according to the DoE methodology proposed in [18, 19]. They were used to understand the noise factors and materi-

al removal mechanisms as well as to select the control factors and their level ranges necessary for the second testing series: the statistical experiments. The process studied is influenced by several parameters. The focus of this work is on: PRF, scanning speed, power, burst mode (number of pulses in a burst) pulse distance (i.e. the distance of two consecutive pulses), line distance and the number of repetitions. A burst is a group of 1 to 8 pulses with a temporal spacing of 12.2 ns ($=1/82\text{ MHz}$). The burst is repeated with the PRF.

Previous experiences show how the pulse repetition frequency has an influence on speed process and pulse energy. The available range of the pulse repetition frequency for the adopted laser system is 50÷8200 kHz, therefore an investigation aiming to find the threshold values was needed. The scanning speed has an influence on speed process and pulse energy, as frequency as well. The maximum value of scanning speed that can be reached by the adopted system is about 2000 mm/s.

Obviously, the power has an influence on removing material process as ablated depth per layer. It is possible to select the desired power percentage ($P_{\%}$). The used laser works in pulse regime. So, the value of pulse distance depends on beam spot and thermal property of the processed material. The line distance is the distance between two consecutive scan lines. It has influence on time process and ablated depth.

The laser system adopted offers a sophisticated and very flexible burst mode. The literature shows (for other kind of materials) that the MRR can be increased by using the burst mode properly [23-25]. In addition, a great advantage in the use of burst mode is that with the same or even higher MRR, the surface roughness can be reduced [25-28].

The number of repetitions represents as often the machined area was fully scanned by laser beam. The influence of this parameter, also indicated as the number of layers (the picosecond laser used machines material layer by layer), on the depth reached is as expected. In fact, if a laser beam travels several times on the same surface the depth of the latter can only increase. In the next experiments this parameter is always hold constant.

For all experiments conducted, the beam was focused at the surface of the workpiece. Before the experiments an ultrasonic cleaning device has been used to clean the sample workpieces. During the tests, local exhaust ventilation was used to facilitate the capture of debris and enhance the surface quality. In addition, during and after the process compressed air has been used to remove dust from the workpiece surface. After machining, the ultrasonic cleaning device and a microfiber cloth have been used in order to remove dust and deposits on the surface.

3.1 Preliminary test

In preliminary tests phase a sample made by Al_2O_3 has been machined with several values of Scanning speed, Power, PRF and line distance.

At first, the research has been focused to identify the critical process parameters for the processing, the operating windows of the process and, then, the values (also referred as levels) adopted by process parameters in the micro structuring test.

In order to find the PRF range of interest, a parameter search matrix was structured on the sample, as it is shown in figure 2. Along the y-axis of the matrix, the PRF was linearly increased from 50 kHz to 8200 kHz with a rise of 905.56 kHz each. Along the x axis of the parameter search matrix, the available power percentage was varied in increments of 10 in a range of 10÷100% at the respective frequency. It results a total of 100 parameter combinations have been examined. In particular, they have been structured 100 pockets with a size of 400 μm per side, as shown in figure 2b. The following constant parameters have been adopted for these tests:

- Pulse distance: $P_d = 3 \mu\text{m}$,
- Line distance: $L_d = 3 \mu\text{m}$,
- Number of repetitions (layers): $R = 50$.

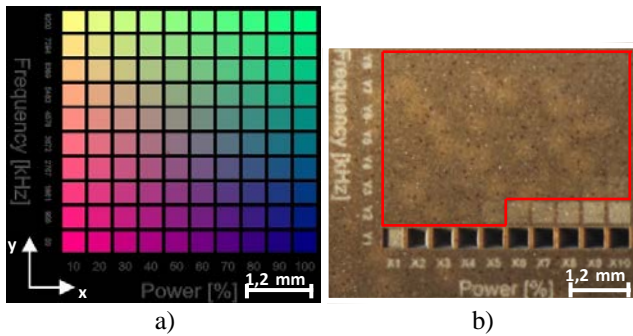


Fig. 2 a) Parameter search mask at PRF range 50÷8.200 kHz. b) Details of sample obtained at PRF range 50÷8.200 kHz.

Figure 2b shows that only in the first lower row the material was ablated. In the second row (PRF = 955,55 kHz) the highest depth (by Power 100 %) was smaller than 1 μm. As a consequence, it is not possible to use a PRF larger than 955 kHz to structure the workpiece surface. However, in the red area the material could not be structured, because the fluence was too low.

In a second time, the PRF has been changed and studied in the range 50÷1000 kHz with a rise of 105,56 kHz. The number of repetition has been set to 20; with this value the reached depths are in the target range of 20÷30 μm. So it is not higher than the rayleigh length of the used laser system. The other parameters (pulse distance, line distance and pocket dimension) were the same as before. The matrix on the sample came out from this experiment is shown in figure 3.

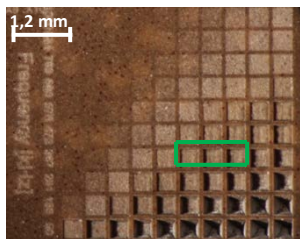


Fig. 3 Details of machining sample at PRF range 50÷1000 kHz.

The results of interest are in the range of PRF = 200÷300 kHz and Power $P\% = 50\div 100\%$. For lower

PRF's the reached depths are too high and the surface quality is too poor. At higher frequencies than 300 kHz, partial bulging was visible on the structural edge.

The best results were achieved with a frequency of 261.55 kHz in the power range of 60÷80 %, highlighted by the green frame in figure 3. Since the depths of the pockets (60 to 200 μm) are interesting for industrial applications, considering the short production time and low surface roughness.

As the available average power depends on the PRF, it is necessary to set the frequency to a value for the final structuring test. Otherwise, the statistical model would be falsified by this noise. The relation between average power available and PRF in the preferred pulse repetition frequency range (200÷300 kHz) is nearly linear:

$$P_{m,av} = -0.039 * PRF + 2.441 \quad (1)$$

The real average power is given from the following formula:

$$P_{m,real} = P_{m,av} * P\% \quad (2)$$

where $P_{m,real}$ is the real average power, $P_{m,av}$ is the available average power and $P\%$ is the percentage power. In order to have full control on the power it is desirable to fix one of the two terms in the second member of last equation. To simplify the power management the pulse repetition frequency has been fixed. The value of pulse repetition frequency chosen has been selected with an appropriate experiment. The previous experiment has shown that the desirable range of depth (i.e. which involves a height of the removed layers nearly 1μm/layer) is obtained when the pulse repetition frequency assumes the value in the range 200÷300 kHz.

Due to an ablation rate of around 1 μm/layer and a low surface roughness in comparison to the other parameter combinations, the setting parameter PRF = 280 kHz, scanning speed = 1675 mm/s and $P\% = 80\%$ were selected as the center point for the experimental design.

In the pretests the burst mode ("Fix Bursts") has been studied, too. In fact, several combinations of parameters with the number of pulses in a burst set to 3 and 5 have been tested. For these settings the reached depth was in a range between 0÷10 μm. The missing ablation occurs because the available power is evenly divided among the number of pulses in a burst. For a Fix B3, for example, this means that its energy corresponds to 1/3 of the energy of a standard pulse. As a result, the pulse energy under the specified boundary conditions is unable to effectively remove material. However, it can still be assumed that the burst mode can lead to an improvement in roughness and MRR. For this, an adaptation of the process parameter area is required. This should be investigated separately in future experiments.

The results of the preliminary test can be summarised as following:

-In order to stabilise the process, it was decided to consider the pulse available average power as a held constant. Therefore, the PRF was fixed at 280 kHz in the present case.

-Too low scanning speeds lead to an increasing process time, which is a conflict of objectives. So, it was decided to investigate the effect of scanning speed near the possible maximum speed of the scanning system, in a range of 1350÷2000 mm/s.

-The depth is affected by the repetition number, which depends on the overall energy released on the filled area. Accordingly, it was decided to adopt the $P_{\%}$ as control factor for the micro structuring tests and the depth per layer as a response variable, because it is linked with the efficiency of the process.

-Finally, the preliminary test has shown that the line distance has a huge influence on the process time. Hence, it was decided to adopt this latter as control factor.

3.2 Design of Experiments

The pre-design analysis and preliminary tests results allowed to define the control factors and their levels (i.e. the process parameters that are setting during the testing phase).

In the present paper, the selected and analysed control factors are: scanning speed, power and line distance.

The latter have been tested realising pockets (400x400 μm^2) with the number of repetition set on 20. The response variables analysed for each pocket are: depth of pocket (measured as average distance between the non-machined surface and the ground of the pocket), arithmetic mean roughness (R_a), average height (R_c), root mean square height (R_q). In this paper they have been discussed only the most interesting variables in order to understand the process: Depth of the pocket and R_a .

Then a Central Composite Design (CCD) was developed and performed in order to understand the influence of main parameters and their interactions on the response variables. The chosen CCD is a centered face plan, with a value of α (distance of the axial points from the center of the plan) set on 1, 2 central points and 6 star points. The plan has been replicated 3 times for a total of 48 runs according with [18].

The setting parameter studied, and their values, are shown in table 2.

Table 2 Control factors and levels adopted in structuring test.

Control factors	Low	Middle	High
Scanning speed [mm/s]	1350	1675	2000
Percentage power [%]	60	80	100
Line distance [μm]	3	6	9

The response variables were measured by a 3D-laser scanning microscope VK 9700 of Keyence, as shown in figure 4.

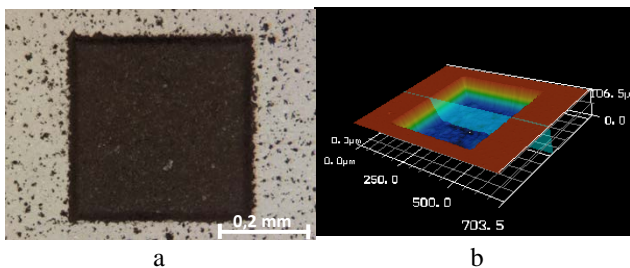


Fig. 4 Pocket of 400 x 400 μm^2 realised on the sample. The figure shows an image of pocket obtained with digital microscope (a). 3-D image of pocket obtained through microscope software management (b).

4. Experimental Results and Discussion

4.1 ANOVA Results

The statistical significance of results has been tested through ANOVA method. In particular, the significance of the control factors scanning speed, $P_{\%}$ and line distance for the Depth, R_a , R_q and R_c response variables has been checked. For each parameter or parameter combination the ANOVA result consists the following information: the degrees of freedom (DF), the adjusted sum of squares (Adj SS), the adjusted mean squares (Adj MS), the f-value and the p-value. The p-value was used to determine the significance of the factors and their combination on the analysed response variables. The analysis was carried out at a 95 % confidence level ($\alpha = 0.05$). Thus, if the p-value is less than 0.05, a process parameter or a parameter interaction is considered significant. The ANOVA hypotheses assumes that the observations are normally and independently distributed with the same variance for each treatment or factor level checked via graphical analysis of residuals [17]. The residuals of each response variable, as shown in figure 5 for depth, have been used to verify that the model provides an adequate approximation of the real system and that none of the hypotheses is violated.

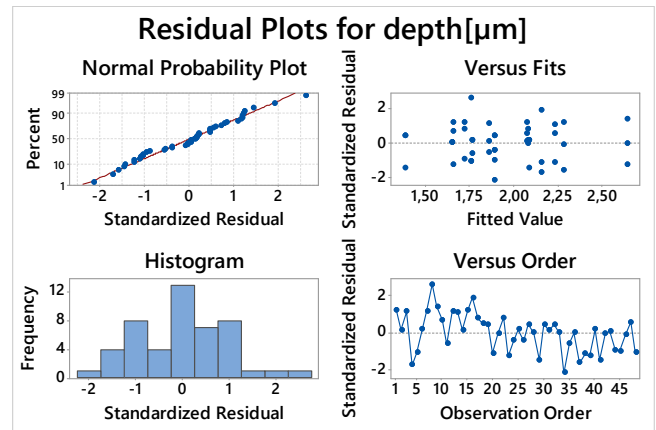


Fig. 5 Residual Plots for depth.

The normality and independence assumption have been verified and the variance of the error is constant.

The ANOVA results are reported in tables 3-4. In the tables, the p-value of each significant effect is highlighted by the bold text.

The ANOVA results for the depth show significance for all the control factors, quadratic effects and their interaction (table 3). The lack of fit is not significant which means that the model correctly specifies the relationship between the response and the predictors. In addition, $S = 0.0089195 \mu\text{m}$ and $R^2 = 99.93 \%$. S represents the standard deviation of the distance between the data values and the fitted values. R^2 is the percentage of variation in the response that is explained by its relationship with one or more predictor variables. So, according with the relevant literature [18] the statistical model quality is good.

The roughness parameters are affected by all the setting parameter chosen (table 4). R_a and R_q show an influence by the interaction $P_{\%} * L_d$.

In the ANOVA tables for the roughness parameters the lack of fit results has been reported too and is not significant. Also for the roughness parameter R_a a good statistical model quality was achieved with $S = 0.18 \mu\text{m}$ and $R^2 = 75.8 \%$.

Table 3 ANOVA for Depth.

Source	Unit	DF	Adj SS	Adj MS	F-Value	P-Value
<u>Model</u>		9	4,21978	0,46886	5893,34	0,000
<u>Linear</u>		3	4,12212	1,37404	17270,8	0,000
Ss	[mm/s]	1	0,73317	0,73317	9215,52	0,000
P%	[%]	1	1,38679	1,38679	17431,0	0,000
Ld	[μm]	1	2,00216	2,00216	25165,9	0,000
<u>Square</u>		3	0,08606	0,02869	360,59	0,000
Ss*Ss		1	0,00490	0,00490	61,61	0,000
P%*P%		1	0,00455	0,00455	57,25	0,000
Ld*Ld		1	0,05491	0,05491	690,15	0,000
<u>2-Way Inter-action</u>		3	0,01159	0,00386	48,57	0,000
Ss*P%		1	0,00589	0,00589	74,04	0,000
Ss*Ld		1	0,00200	0,00200	25,09	0,000
P%*Ld		1	0,00371	0,00371	46,57	0,000
Error		38	0,00302	0,00008		
Lack-of-Fit		5	0,00031	0,00006	0,77	0,581
Pure Error		33	0,00271	0,00008		
Total		47	4,22280			

Table 4 ANOVA for R_a .

Source	Unit	DF	Adj SS	Adj MS	F-Value	P-Value
<u>Model</u>		9	3,78675	0,42075	12,87	0,000
<u>Linear</u>		3	3,22776	1,07592	32,92	0,000
Ss	[mm/s]	1	0,14434	0,14434	4,42	0,042
P%	[%]	1	2,28890	2,28890	70,02	0,000
Ld	[μm]	1	0,82043	0,82043	25,10	0,000
<u>Square</u>		3	0,15848	0,05283	1,62	0,202
Ss*Ss		1	0,00043	0,00043	0,01	0,909
P%*P%		1	0,00043	0,00043	0,01	0,909
Ld*Ld		1	0,12509	0,12509	3,83	0,058
<u>2-Way Inter-action</u>		3	0,56750	0,18917	5,79	0,002
Ss*P%		1	0,00064	0,00064	0,02	0,889
Ss*Ld		1	0,04535	0,04535	1,39	0,246
P%*Ld		1	0,53179	0,53179	16,27	0,000
Error		37	1,20942	0,03269		
Lack-of-Fit		5	0,18109	0,03622	1,13	0,366
Pure Error		32	1,02833	0,03214		
Total		46	4,99617			

In figures 6-7 the main effect plots of the depth and R_a are shown respectively.

The interaction plots are shown in figures 8-9.

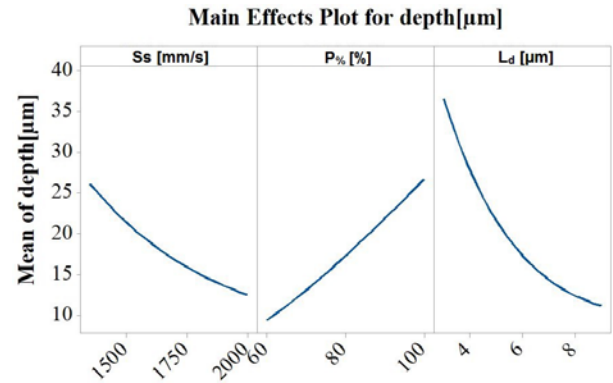


Fig. 6 Main effects plots for depth.

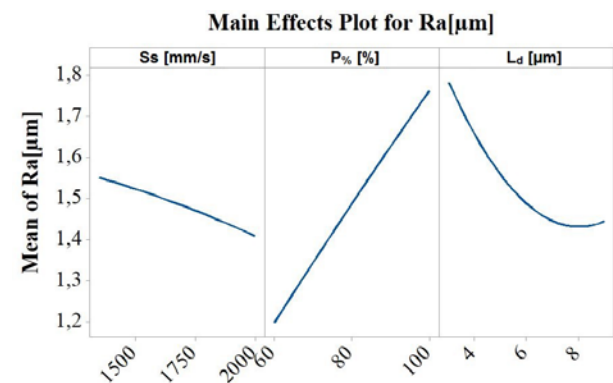


Fig. 7 Main effects plots for R_a .

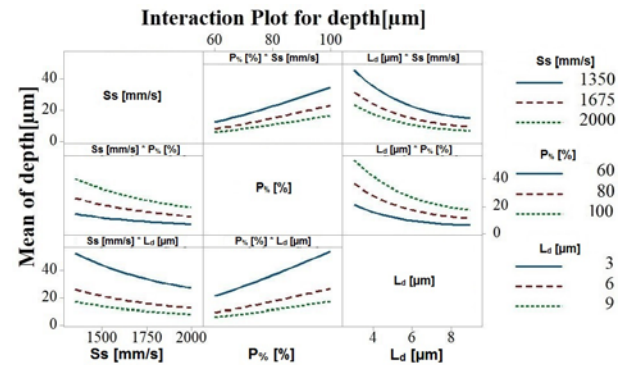


Fig. 8 Interaction plots for depth.

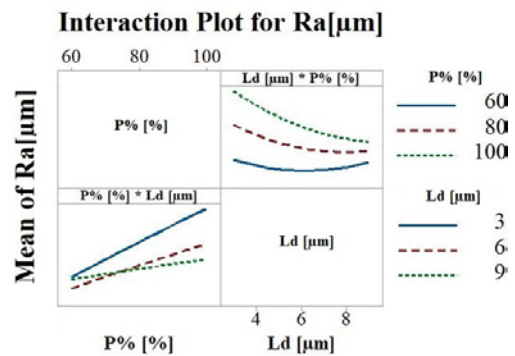


Fig. 9 Interaction plots for R_a .

4.2 Influence of Scanning Speed

The scanning speed has influence on the local warming at the workpiece surface. Scanning speed is linked with pulse repetition frequency through the following formula:

$$S_s = P_d * PRF \tag{3}$$

If scanning speed decreases the pulse distance will decrease, because the PRF is fixed at 280 kHz. Moreover, the interaction time with the material will increase and the local temperature will increase, too. In this case, the achievable depth increases as the energy required to vaporise the material decreases, as shown in figure 6. These aspects do conform what is observed in Leone et al. in [1].

As a result of the lower P_d , the pulse overlap increases. The pulse overlaps causes a re-worked surface which worsen the roughness, as it is reported in figure 7.

4.3 Influence of Power

As expected the $P_{\%}$ affects the pocket depth that is nearly directly proportional to the released power, as shown in figure 6. As is known, the power is linked with the fluence. An appropriate relation between the fluence and depth reached is described by the formula [20]:

$$z_{abl} = \delta * \ln (F/F_{th}) \tag{4}$$

where z_{abl} is the ablation depth, δ is the penetration depth, F_{th} is the threshold fluence and F the fluence. So it is clear: if the power increases, the fluence F of the laser pulse will rise and the ablation depth also will go up.

The main effects plot for R_a in figure 7 shows a strong relation between power and roughness: when power increases the roughness gets worse. This behavior is due to the increase in fluence that occurs when power increases. If the latter increases, the ablation depth will rise too. The increase of roughness with depth can be partly explained by debris re-deposition that affects the developing surface, [22, 29]. In figure 10 the machined surface of the workpiece and the re-deposited debris is shown in detail, by a scanning electron microscopy (SEM).

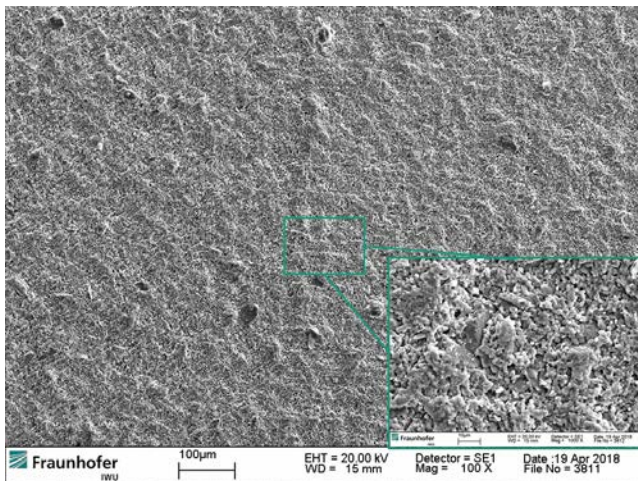


Fig. 10 SEM of microstructure surface machined with $S_s = 1350$ mm/s; $P_{\%} = 100$ % and $L_d = 3$ μ m.

To ensure that the re-solidified particles on the workpiece surface, are material deposits, an EDX analysis was executed. Figure 11 shows re-solidified particles on the workpiece surface. The results are summarised in table 5.

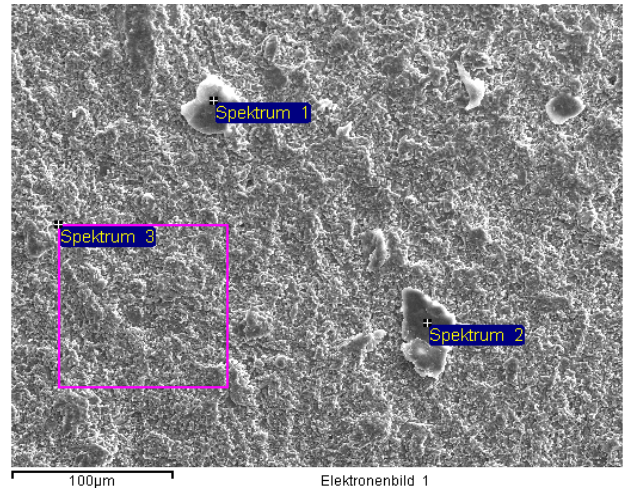


Fig. 11 SEM of microstructure surface machined with $S_s = 1350$ mm/s; $P_{\%} = 100$ % and $L_d = 3$ μ m.

Table 5 Results of the structured surface EDX analysis ($S_s = 1350$ mm/s; $P_{\%} = 100$ % and $L_d = 3$ μ m).

Spectrum	O [wt. %]	Na [wt. %]	Al [wt. %]	Si [wt. %]	Cl [wt. %]	K [wt. %]	Ca [wt. %]	Ti [wt. %]	Mn [wt. %]	Σ [wt. %]
1	59	12.9	5.0	-	17.4	5.5	-	-	-	100
2	47	4.8	11.1	4.5	8.8	4.6	18.8	-	-	100
3	36	0.4	57.4	1.0	-	0.3	-	1.1	3.2	100
SM	35	-	60.5	0.6	-	-	-	1.2	2.5	100

The comparison with the starting material (spectrum SM in table 5) shows that the particles are re-deposited material particles. Especially, spectrum 3 has a high agreement with the starting material. Spectrum 1 and 2 contain elements that are not constituents of alumina. This is attributed to impurities. In the course of processing with the picosecond laser, the oxygen content in the material is slightly increased.

4.4 Influence of Line Distance

The line distance is significant for the analysed response variables. If L_d increases, depth and surface roughness will decrease, as shown in figures 6-7. The effect of L_d on depth could be explained similarly to the effect of the scanning speed: if L_d decreases, the distance between the filling lines will drop and the number of scan lines will increase. Following to this, more pulses to ablate material are achieved and the depth will rise. Furthermore, the average temperature of the pocket will increase [1]. Consequently, by fixed power, the depth rises at the L_d decreases (figure 8).

The growing of roughness is associated with the increase of material removed and re-solidified. When the line distance increases, the ablation capability decreases and the amount of material that can re-solidified also decreases. Furthermore, when line distance drops the number of hits at the surface increase and debris respectively roughness can only rise.

It is expected that the effect of L_d on roughness will decrease with increasing structural dimensions as the time interval between two consecutive scan lines increases.

Moreover, ANOVA tables 4-6 indicate the presence of a significant interaction between L_d and power for the response variable roughness (figure 9). If the power goes up, the obtained roughness is influenced by the chosen line distance level. In particular, if the power increases and line distance is set on a high value the roughness will rise slowly because the ablation capability is not too high. If L_d is set on a low value, the roughness will go up fast by increasing power. In fact, the total energy density, at the same power, decreases if line distance increases [1]:

$$E_t = (P_m * R)/(L_d * Ss) \quad (5)$$

where E_t is the total energy density, P_m is the mean beam power, R the number of repetitions and Ss the scanning speed.

5. Response Surfaces

The Central Composite Design allows to perform an appropriate forecasting model. In fact, a quadratic regression model has been performed for each response. The latter allow us to analyse combinations of parameter not tested yet.

In particular, the regression models for the analysed depth of pocket and R_a are as follows:

$$\begin{aligned} \text{Depth}^{0,22293} &= 2,6336 + (-0,001134 Ss) & (6) \\ &+ 0,02563 P\% + (-0,19631 L_d) \\ &+ (-0,000060 P\%^2) + 0,009258 L_d^2 \\ &+ (-0,000002 Ss * P\%) \\ &+ 0,000009 Ss * L_d \\ &+ (-0,000207 P\% * L_d) \\ R_a &= -0,54 + 0,00036 Ss + 0,0337 P\% + & (7) \\ &(-0,056 L_d) + (-0,002550 P\% * L_d) \end{aligned}$$

Through contour and surface plots the local shape of the response surface can be graphically studied. They show how the response varies as a function of two factors at a time, while averaging over the others. Furthermore, the CCD is useful to find the optimum working condition to obtain a specific target performance. The regression equation can be studied graphically through the response surface. The surfaces in figure 12-14 plot the response variable R_a for each couple of setting parameters where the third parameter is set on the middle value.

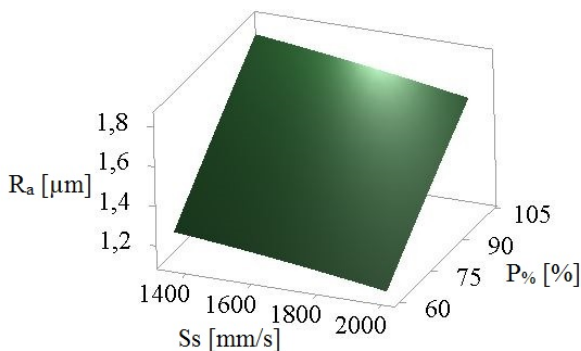


Fig. 12 Surface plot of R_a vs $P\%$ - Ss .

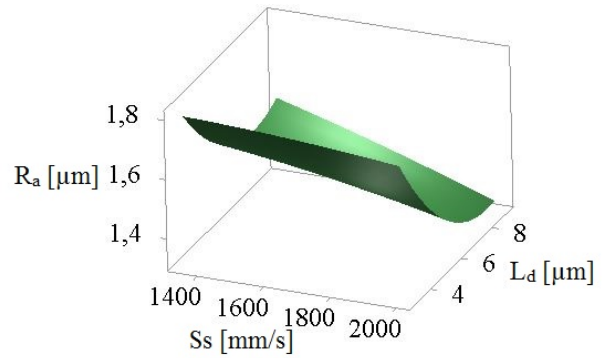


Fig. 13 Surface plot of R_a vs L_d - Ss .

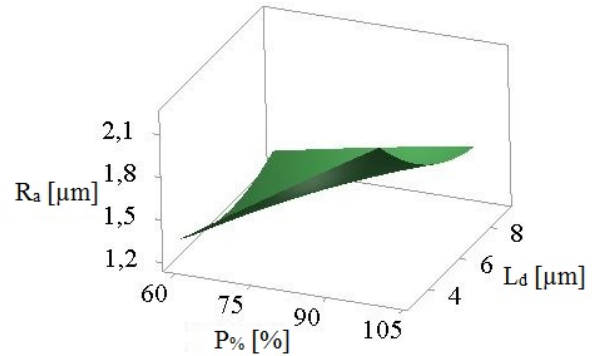


Fig. 14 Surface plot of R_a vs $P\%$ - L_d .

It is clear how R_a does change for every interaction of the factors.

Moreover, through the response surface it is possible to locate the area that identifies the maximum value of roughness. The projection on plane of a response surface is a contour plot. In figure 15, following the colorimetric scale, it possible to observe areas where the roughness takes higher value (dark green) and lower (dark blue).

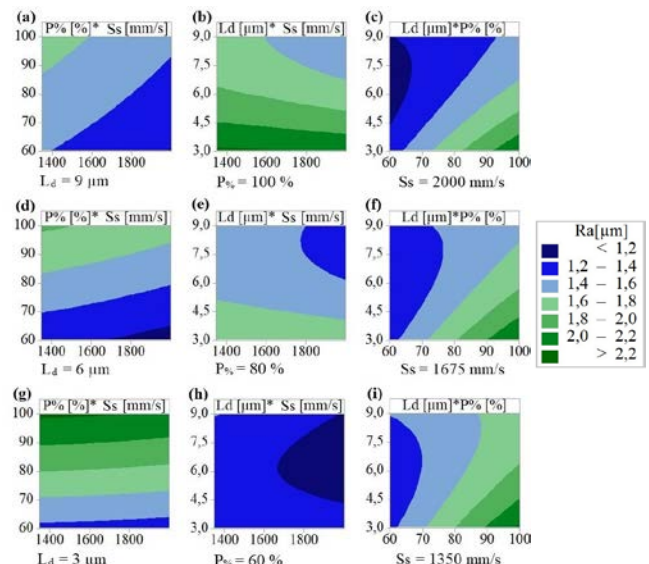


Fig. 15 Contour plot for R_a with third parameter set on low, middle and high level.

In figure 15 there is an overview of the roughness value for each combination of the factors.

In example, when percentage power is set on the low level the roughness value does not exceed 1.4 μm for any other combination of scanning speed and line distance (in the tested range of values), as is visible in the plot of figure 15 (h).

The same analysis has been performed on the response variable depth, as shown in figure 16.

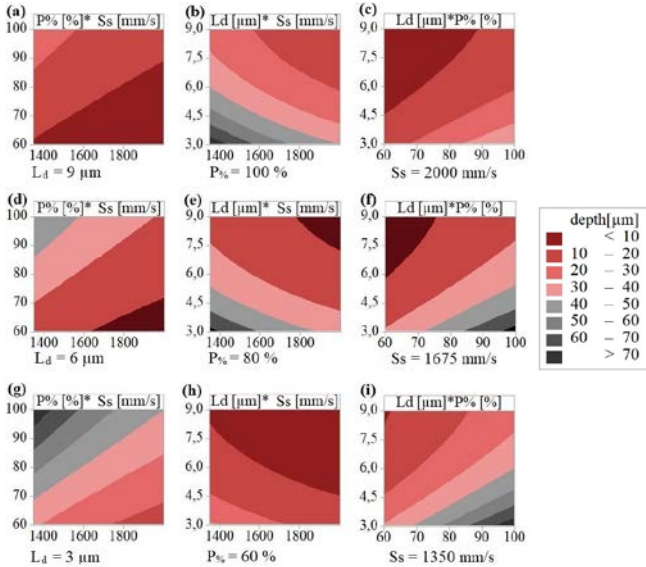


Fig. 16 Contour plot for depth with third parameter set on low, middle and high level.

6. Optimisation Step

The statistical approach allows optimising process parameters for more than one response variable simultaneously, performing a multi-response optimisation (MRO). The latter finds the setting parameters that provide the “most desirable” response values. [30]

In general, for each response variable Y_i , a desirability function d_i (with $0 \leq d_i(Y_i) \leq 1$) assign a number onto a [0,1] scale, where 1 is the most desirable value and 0 is unacceptable. To simultaneously optimise all the responses Y_i , all the individual desirability d_i are combined in an overall desirability function Df . The optimisation is achieved where the Df is maximised. [30] In this work, the method proposed has been used for the two variables depth of pocket and R_a . So, it results:

$$Df = (d_1^{w_1} \times d_2^{w_2})^{1/(w_1+w_2)} \tag{8}$$

where w_1 and w_2 are the response weights.

The main objective of the study was to develop a sustainable and efficient micro structuring process.

The regression model built up allows to find the setting parameters for a fixed target. For example, it has been searched the setting parameters which removed 1 μm/layer and minimise R_a . The regression model has been built fixing the number of layer to 20, so a depth per layer of 1μm/layer will be reached if a depth of 20 μm will be reached too. The regression model has been consulted through a statistical software, and the result is shown in figure 17. Furthermore, the L_d has been set on 8 μm in order to reduce the time required for the ablation process.

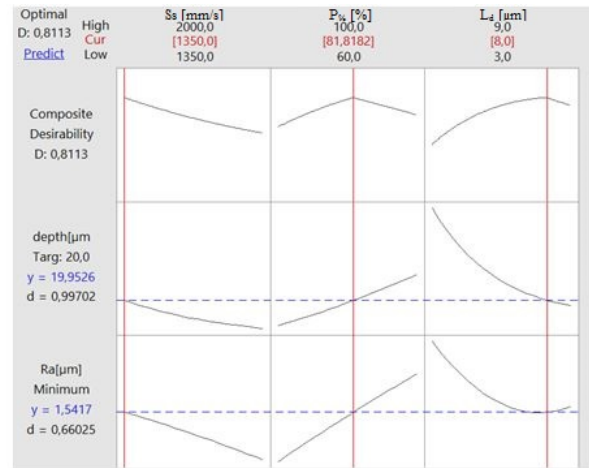


Fig. 17 Optimisation plot for the boundary conditions ablation rate = 1 μm/layer and minimise R_a .

Figure 17 shows the optimisation plot in which is reported the effect of each factor (columns) on the responses or composite desirability (rows). Composite desirability is the weighted geometric mean of the individual desirability for the responses [18] and evaluates how the settings optimise a set of responses overall

The setting parameter have been used in order to obtain an ablation of 34 μm, the results are shown in table 6.

Table 6 Tested optimisation parameters and results.

Setting parameters	Process time [min]	R_a [μm]	Depth [μm]
$S_s = 1350$ mm/s; $P\% = 81$ %; $L_d = 8$ μm	3:27	1.541	36.95

The difference between the depth obtained and target is about 2.9 μm. These results indicate that the parameters chosen remove 1.087 μm/layer, result near the target value of 1 μm/layer.

It was worked at high fluences to achieve the required process times. As a result, the roughness could indeed be reduced, but it is still high. Optimisation approaches are therefore seen in the analysis of lower fluences as well as in the deeper testing of the burst mode.

7. Conclusion

In this work, a CCD for laser micro structuring process on aluminum oxide has been performed according to the DoE methodology.

First of all, the CCD detected which process parameters affect the process and how they do it.

Furthermore, thanks to the analysis of results, a forecasting quadratic regression model, for the chosen response variables, has been developed. The model defines the response variables behaviour in the experimented parameters domain.

Moreover, the use of an optimisation tool, as the adopted desirability function, enables to control the process. In fact, the desirability function suggests the appropriate process parameter setting in order to obtain the desired results in terms of depth and roughness.

So, with the regression models, fixing a target values for the response variables, it is possible to find the setting parameters that provide these targets.

References

- [1] C. Leone, S. Genna, F. Tagliaferri, B. Palumbo, M. Dix: Experimental investigation on laser milling of aluminium oxide using a 30W Q-switched Yb:YAG fiber laser, *Optics & Laser Tech.*, 76, (2016) 127.
- [2] I. P. Tuersley, A. Jawaid, I.R. Pashby: Review: Various methods of machining advanced ceramic materials, *J. Mater. Process. Tech.*, 42/4, (1994) 377.
- [3] A. Sabur, M. Y. Ali, Md. A. Maleque, A. A. Khan: Investigation of material removal characteristics in EDM of nonconductive ZrO₂ ceramic, *Proc. Eng.*, 56, (2013) 696.
- [4] F. Calignano, L. Denti, E. Bassoli, A. Gatto, L. Iuliano: Studies on electrodischarge drilling of an Al₂O₃-TiC composite, *Int. J. Adv. Manuf. Tech.*, 66/9-12, (2013) 1757.
- [5] Y. X. Feng, C. Z. Huang, J. Wang, X. Y. Lu, H. T. Zhu: Surface characteristics of ceramics milled with abrasive waterjet technology, *Key Eng. Mater.*, 329, (2007) 335.
- [6] Y. X. Feng, C. Z. Huang, J. Wang, R. G. Hou, X. Y. Lu: An experimental study on milling Al₂O₃ ceramics with abrasive waterjet, *Key Eng. Mater.*, 339, (2007) 500.
- [7] J. Zeng, T. J. Kim: An erosion model of polycrystalline ceramics in abrasive waterjet cutting, *Wear*, 193/2, (1996) 207.
- [8] M. Dittrich, M. Dix, M. Kuhl, B. Palumbo, F. Tagliaferri: Process analysis of water abrasive fine jet structuring of ceramic surfaces via design of experiment, *Procedia CIRP*, 14, (2014) 442.
- [9] F. Tagliaferri, M. Dittrich, B. Palumbo: "A Systematic Approach to Design of Experiments in Waterjet Machining of High Performance Ceramics" ed. by J. P. Davim (Springer, Cham, 2016) 109.
- [10] K.-H. Leitz, B. Redlingshöfer, Y. Reg, A. Otto, M. Schmidt: Metal Ablation with Short and Ultrashort Laser Pulses, *Phys. Proc.*, 12, (2011) 230.
- [11] S. Mishra, V. Yadava: Laser beam MicroMachining (LBMM)-A review, *Optics & Laser in Eng.*, 73, (2015) 89.
- [12] C. Leone, V. Lopresto, I. De Iorio: Wood engraving by Q-switched diode pumped frequency doubled Nd:YAG green laser, *Optics & Laser in Eng.*, 47/1, (2009) 161.
- [13] C. Leone, I. Papa, F. Tagliaferri, V. Lopresto: Investigation of CFRP laser milling using a 30W Q-switched Yb:YAG fiber laser: effect of process parameters on removal mechanisms and HAZ formation, *Compos. Part A: Appl. Sci. Manuf.*, 55, (2014) 129.
- [14] S. Guarino, G. Ponticelli, O. Giannini, S. Genna, F. Trovalusci: Laser milling of Yttria-Stabilized-Zirconia by using a Q-Switched Yb:YAG fiber laser: experimental analysis, *Int. J. Adv. Manuf. Tech.*, 94/1-4, (2018) 1373.
- [15] V. Semak, A. Matsunawa: The role of recoil pressure in energy balance during laser materials processing, *J. Phys. D: Appl. Phys.*, 30/18, (1997) 2541.
- [16] D. Perez, L. J. Lewis: Thermodynamic evolution of materials during laser ablation under pico and femto-second pulses, *Appl. Phys. A: Mater. Sci. Process.*, 79/4-6, (2004) 987.
- [17] S. P. Harimkar, A. N. Samant, N. B. Dahotre: Temporally evolved recoil pressure driven melt infiltration during laser surface modifications of porous alumina ceramic, *J. Appl. Phys.*, 101, (2007) 054911.
- [18] D. C. Montgomery: "Design and Analysis of Experiments" (Wiley, New York, 2012).
- [19] D. E. Coleman, D. C. Montgomery: A systematic approach to planning for a designed industrial experiment, *Technometrics*, 35/1, (1993) 1.
- [20] B. Jaeggi, B. Neuenschwander, M. Schmid, M. Muralt, J. Zuercher, U. Hunziker: Influence of the Pulse Duration in the ps-Regime on the Ablation Efficiency of Metals, *Phys. Proc.*, 12, (2011) 164.
- [21] B. C. Chen, C. Y Ho, M. Y. Wen, C. S. Chen, C. Mab, Y. H. Tsai: Ultrashort-laser-pulse machining characteristics of aluminum nitride and aluminum oxide, *Cer. Int.*, 41/1, (2015) S191.
- [22] W. Perrie, A. Rushton, M. Gill, P. Foxa, W. O'Neill: Femtosecond laser micro-structuring of alumina ceramic, *Appl. Sur. Sci.*, 248/1-4, (2005) 213.
- [23] W. Hu, Y. C. Shin, G. King: Modeling of multi-burst mode pico-second laser ablation for improved material removal rate, *Appl. Phys. A: Mater. Sci. & Process.*, 98/2, (2009) 407.
- [24] P. Lickschat, A. Demba, S. Weissmantel: Ablation of steel using picosecond laser pulses in burst mode, *Appl. Phys. A: Mater. Sci. & Process.*, 123/2, (2017) 137.
- [25] C. Emmelmann, J. Urbina: Analysis of the Influence of Burst-Mode Laser Ablation by Modern Quality Tools, *Phys. Proc.*, 12, (2011) 172.
- [26] B. Neuenschwander, T. Kramer, B. Jaeggi: Burst mode with ps- and fs-pulses: Influence on the removal rate, surface quality and heat accumulation, *Proceedings of SPIE*, 9350, (2015) 93500U-1.
- [27] R. Knappe, H. Haloui, A. Seifert, A. Nebel: Scaling ablation rates for picosecond lasers using burst micromachining, *Proceedings of SPIE*, 7585, (2010) 7585H-1.
- [28] M. Vogel: „Untersuchung des Einflusses von Laser-Burst's auf die Abtragsqualität und das Abtragsvolumen“ (Technische Universität Chemnitz, Chemnitz, 2017).
- [29] M. Mendes, V. Oliveira R. Vilar, F. Beinhorn, J. Ihlemann, O. Conde: XeCl laser ablation of Al₂O₃-TiC ceramics, *Appl. Sur. Sci.*, 154-155, (2000) 29.
- [30] S. Genna, F. Tagliaferri, I. Papa, C. Leone, B. Palumbo: Multi-Response Optimization of CFRP Laser Milling Process Based on Response Surface Methodology, *Polymer Eng. & Sci.*, 57/6, (2017) 595.

(Received: June 22, 2018, Accepted: August 26, 2018)